CAMBRIDGE
UNIVERSITY PRESS

Article

Princivalleite, Na(Mn$_2$Al)Al$_6$(Si$_6$O$_{18}$)(BO$_3$)$_3$(OH)$_3$O, a new mineral species of the tourmaline supergroup from Veddasca Valley, Varese, Italy

Ferdinando Bosi[1]* , Federico Pezzotta[2], Henrik Skogby[3], Alessandra Altieri[1] , Ulf Hålenius[3],

Gioacchino Tempesta[4] and Jan Cempírek[5]

[1]Department of Earth Sciences, Sapienza University of Rome, Piazzale A. Moro, 5, I-00185 Rome, Italy; [2]Natural History Museum, Corso Venezia 55, 20121 Milan, Italy; [3]Department of Geosciences, Swedish Museum of Natural History, Box 50007, SE-10405 Stockholm, Sweden; [4]Dipartimento di Scienze della Terra e Geoambientali, Università degli Studi di Bari Aldo Moro, Bari, Italy; and [5]Department of Geological Sciences, Faculty of Science, Masaryk University, Kotlářská 2, 611 37, Brno, Czech Republic

Abstract

Princivalleite, Na(Mn$_2$Al)Al$_6$(Si$_6$O$_{18}$)(BO$_3$)$_3$(OH)$_3$O, is a new mineral (IMA2020-056) of the tourmaline supergroup. It occurs in the Veddasca Valley, Luino area, Varese, Lombardy, Italy (46°03'30.74"N, 8°48'24.47"E) at the centre of a narrow (2–3 cm wide) vertical pegmatitic vein, a few metres long, crosscutting a lens of flaser gneiss. Crystals are subhedral (up to 10 mm in size), azure with a vitreous lustre, conchoidal fracture and white streak. Princivalleite has a Mohs hardness of ~7, a calculated density of 3.168 g/cm^3 and is uniaxial (–). Princivalleite has trigonal symmetry, space group $R3m$, $a = 15.9155(2)$ Å, $c = 7.11660(10)$ Å, $V = 1561.15(4)$ Å^3 and $Z = 3$. The crystal structure was refined to $R_1 = 1.36\%$ using 1758 unique reflections collected with Mo$K\alpha$ X-ray intensity data. Crystal-chemical analysis resulted in the empirical crystal-chemical formula
^{X}(Na$_{0.54}$Ca$_{0.11}\square_{0.35}$)$_{\Sigma1.00}$^{Y}(Al$_{1.82}$Mn$^{2+}_{0.84}$Fe$^{2+}_{0.19}$Zn$_{0.07}$Li$_{0.08}$)$_{\Sigma3.00}$^{Z}(Al$_{5.85}$Fe$^{2+}_{0.13}$Mg$_{0.02}$)$_{\Sigma6.00}$[^{T}(Si$_{5.60}$Al$_{0.40}$)$_{\Sigma6.00}$O$_{18}$](BO$_3$)$_3$$^{O(3)}$[(OH)$_{2.71}O_{0.29}$]$_{\Sigma3.00}$ $^{O(1)}$[O$_{0.66}$F$_{0.22}$(OH)$_{0.12}$]$_{\Sigma1.00}$ which recast in its ordered form for classification purposes is:
^{X}(Na$_{0.54}$Ca$_{0.11}\square_{0.35}$)$_{\Sigma1.00}$^{Y}(Al$_{1.67}$Mn$^{2+}_{0.84}$Fe$^{2+}_{0.32}$Zn$_{0.07}$Mg$_{0.02}$Li$_{0.08}$)$_{\Sigma3.00}$^{Z}Al$_{6.00}$[^{T}(Si$_{5.60}$Al$_{0.40}$)$_{\Sigma6.00}$O$_{18}$](BO$_3$)$_3$^{V}[(OH)$_{2.71}$O$_{0.29}$]$_{\Sigma3.00}$ ^{W}[O$_{0.66}$F$_{0.22}$(OH)$_{0.12}$]$_{\Sigma1.00}$.

Princivalleite is an oxy-species belonging to the alkali group of the tourmaline supergroup. The closest end-member compositions of valid tourmaline species are those of oxy-schorl and darrellhenryite, to which princivalleite is related by the substitutions Mn^{2+} ↔ Fe^{2+} and Mn^{2+} ↔ 0.5Al^{3+} + 0.5Li$^+$, respectively. Princivalleite from Veddasca Valley is a geochemical anomaly, originated in a B-rich and peraluminous anatectic pegmatitic melt formed *in situ*, poor in Fe and characterised by reducing conditions in the late-stage metamorphic fluids derived by the flaser gneiss. The Mn-enrichment in this new tourmaline is due to absence of other minerals competing for Mn such as garnet.

Introduction

Tourmalines are complex borosilicates that have been studied extensively in terms of their crystal structure and crystal chemistry (e.g. Foit, 1989; Hawthorne, 1996; Hawthorne and Henry, 1999; Ertl *et al.*, 2002; Novák *et al.*, 2004; Bosi and Lucchesi, 2007; Bosi, 2013, 2018; Henry and Dutrow, 2011; Cempírek *et al.*, 2013; Bačík and Fridrichová, 2020). In accordance with Henry

*Author for correspondence: Ferdinando Bosi, Email: ferdinando.bosi@uniroma1.it

et al. (2011), the general chemical formula of tourmaline is written as: XY$_3$Z$_6$T$_6$O$_{18}$(BO$_3$)$_3$V$_3$W, where X = Na$^+$, K$^+$, Ca^{2+}, $\square$ (= vacancy); Y = Al^{3+}, Fe^{3+}, Cr^{3+}, V^{3+}, Mg^{2+}, Fe^{2+}, Mn^{2+}, Li$^+$; Z = Al^{3+}, Fe^{3+}, Cr^{3+}, V^{3+}, Mg^{2+}, Fe^{2+}; T = Si^{4+}, Al^{3+}, B^{3+}; B = B^{3+}; V = (OH)$^-$, O^{2-}; and W = (OH)$^-$, F$^-$, O^{2-}. Note that the non-italicised letters X, Y, Z and B represent groups of cations hosted in the $^{[9]}$X, $^{[6]}$Y, $^{[6]}$Z, $^{[4]}$T and $^{[3]}$B crystallographic sites (letters italicised). As for the letters V and W, they represent groups of anions accommodated at the [3]-coordinated O3 and O1 crystallographic sites, respectively. The dominance of specific ions at one or more sites of the structure gives rise to a range of distinct mineral species.

A formal description of the new tourmaline species princivalleite is presented here. The mineral is named after Francesco

Fig. 1. Photo of the azure princivalleite in reflected light: crystalline aggregates in pegmatitic vein in gneiss. Field of view ca. 12 cm × 12 cm. Sample deposited in the collections of the Natural History Museum of Milano, Italy (photo by F. Pezzotta).

Princivalle (b. 1956), Professor of Mineralogy at the Department of Mathematics and Geosciences, University of Trieste, Italy, for his contributions to the understanding of the crystal chemistry and geothermometery of several group minerals such as spinels, olivines and pyroxenes. The new species and the name (symbol Pva) have been approved by International Mineralogical Association's Commission on New Minerals, Nomenclature and Classification (IMA2020-056, Bosi *et al.*, 2020). Holotype material is deposited in the collections of the Natural History Museum of Milano, Italy, catalogue number M38850.

Occurrence

The holotype specimen was collected in 2003 by one of the authors (FP), along the cut of a small road at the eastern side of the Curiglia Village, Veddasca Valley, Luino area, Varese, Lombardy, Italy (46°03′30.74″N, 8°48′24.47″E, ∼730 m above the sea level). The Veddasca Valley is characterised by rocks belonging to the 'Serie del Laghi', a structural unit which is part of the tectonic unit known as Massiccio del Laghi, comprising the central-western sector of the crystalline basement of the Southern Alps (Pezzotta and Pinarelli, 1994). The 'Serie dei Laghi' consists of paragneiss (pelites, sandstones, greywackes and metatufites) and scattered orthogneissic bodies, affected by amphibolite-facies Hercynian metamorphism (Boriani *et al.*, 1990).

During a detailed field mapping performed by one of the authors in 1990–1991, a few narrow, not-metamorphic, veins of pegmatite were discovered nearby the Curiglia village in the Veddasca valley. These pegmatites, which have never been reported in literature, crosscut some heavily deformed metamorphic rocks (flaser gneiss) perpendicularly to their foliation, and probably originated by some minor partial melting that occurred during the uplift of the tectonic units, during the latest stages of the Hercynian metamorphic event. At the centre of one

of these small veins (2 to 3 cm wide and a few metres long), vertically crosscutting the flaser gneiss at Curiglia, there are some quite common occurrences of dispersed grains and crystals up to 1 cm long, of azure princivalleite and oxy-schorl. The pegmatitic vein is composed of muscovite aggregates, with blades mostly oriented perpendicular to the walls, with quartz, albitic plagioclase and minor K-feldspar. In addition to tourmaline, other accessories are rare small pyrite crystals and violet glassy cordierite grains.

Appearance, physical and optical properties

The princivalleite crystals show subhedral habits, up to ∼10 mm and are azure with a vitreous lustre (Fig. 1). It has a white streak and shows no fluorescence. It has a Mohs hardness of ∼7 and is brittle with a conchoidal fracture. The calculated density, based on the empirical formula and unit-cell volume refined from single-crystal X-ray diffraction (XRD) data, is 3.168 g/cm^3. In thin section, princivalleite is transparent; in transmitted light, pleochroism was not visible in the thin-section fragment investigated. Princivalleite is uniaxial (–) with refractive indices $\omega = 1.650(5)$ and $\varepsilon = 1.635(5)$ measured by the immersion method using white light from a tungsten source. The mean index of refraction, density, and chemical composition led to an excellent compatibility index $(1 - Kp/Kc = 0.024)$ (Mandarino, 1981).

Experimental methods and results

General comment

The present crystal structure refinement (SREF), electron microprobe (EMP) and μ-laser induced breakdown spectroscopy (μ-LIBS) data were all obtained from the same crystal fragment. However, complementary experimental data were recorded from coexisting crystals. Small differences in composition occur between these princivalleite crystals (see text).

Microprobe analysis

Electron microprobe analysis was obtained using a wavelength dispersive spectrometer (WDS mode) with a Cameca SX50 instrument at the 'Istituto di Geologia Ambientale e Geoingegneria (Rome, Italy), CNR', operating at an accelerating potential of 15 kV, a sample current of 15 nA and 10 μm beam diameter. Minerals and synthetic compounds were used as standards: wollastonite (Si and Ca), magnetite (Fe), rutile (Ti), corundum (Al), vanadinite (V) fluorophlogopite (F), periclase (Mg), jadeite (Na), orthoclase (K), sphalerite (Zn), rhodonite (Mn) and metallic Cr and Cu. The PAP routine was applied (Pouchou and Pichoir, 1991). The composition (mean of 6 spot analyses) is given in Table 1. Titanium, V, Cr and K were below detection limits (<0.03 wt.%).

Micro-laser induced breakdown spectroscopy

Lithium analysis was performed using 110 mJ of energy per pulse by a double pulse Q-Switched (Nd-YAG, λ = 1064 nm) laser with a 1 μs delay between the two pulses. The small spot size (7–10 μm) was obtained using a petrographic optical microscope (objective lens = 10X, NA = 0.25 and WD = 14.75 mm). The μ-LIBS spectra were acquired using an AvaSpec Fiber Optic Spectrometer (390–900 nm with 0.3 nm resolution) with a delay of 2 μs after the second pulse

Table 1. Electron microprobe data (WDS mode) and atoms per formula unit (apfu) normalised to 31 anions for princivalleite.

Wt.%	Mean (6 spots)	Range	Stand. Dev.	apfu
SiO_2	33.71	33.21–34.10	0.37	5.60
B_2O_3[a]	10.46			3.00
Al_2O_3	41.19	39.32–42.82	1.20	8.07
FeO[b]	2.29	1.85–2.69	0.36	0.32
MnO	5.96	5.46–6.00	0.43	0.84
MgO	0.08	0.04–0.12	0.03	0.02
ZnO	0.55	0.43–0.61	0.08	0.07
CaO	0.60	0.50–0.75	0.12	0.11
Na_2O	1.68	1.59–1.78	0.08	0.54
Li_2O[c]	0.12	0.11–0.13	0.02	0.08
F	0.42	0.35–0.63	0.13	0.22
H_2O[a]	2.55			2.83
O = F	–0.18			
Total	99.45			

[a]Calculated by stoichiometry, (Y+Z+T) = 15.00 apfu.
[b]Fe oxidation state determined by Mössbauer spectroscopy.
[c]Li Determined by µ-Laser Induced Breakdown Spectroscopy.

Fig. 2. Mössbauer spectrum of princivalleite. Fitted absorption doublets assigned to Fe^{2+} are indicated in blue colour. Diamonds denote measured spectrum, and black curve represents summed fitted spectra.

and were integrated for 1 ms. Quantitative data were obtained by generating a linear regression using the main Li emission line intensity (670.706 nm corresponding to resonance transition $1s^2 2s > 1s^2 2p$) particularly sensitive to Li amounts. The linear fit was made according to Bosi *et al.* (2021) and revealed amounts of Li_2O = 0.12 wt.% (Table 1) in line with that estimated by the Pesquera *et al.* (2016) approach (0.18 Li_2O wt.%).
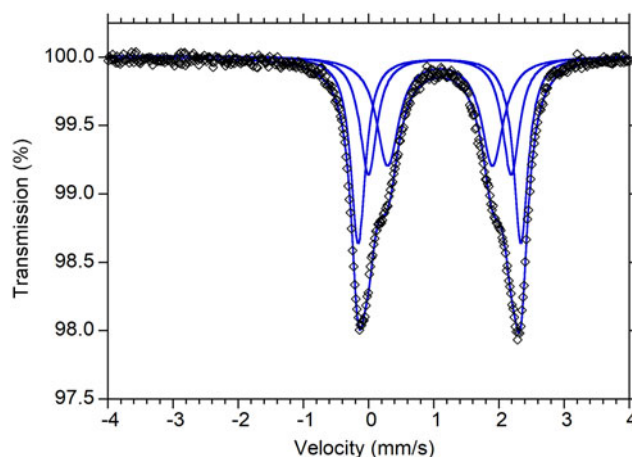
Mössbauer spectroscopy

To determine the $Fe^{3+}/\Sigma Fe$ ratio of princivalleite, a crystal fragment was ground under acetone and analysed using ^{57}Fe Mössbauer spectroscopy with a conventional spectrometer system equipped with a 10 mCi point source and operated in constant acceleration mode. Data were collected over 1024 channels and were folded and calibrated against the spectrum of an α-Fe foil. The spectrum (Fig. 2) was fitted using the software *MossA* (Prescher *et al.*, 2012) with three absorption doublets consistent with Fe^{2+} (Table 2). No indications of absorption due to Fe^{3+} was observed.

Single-crystal infrared spectroscopy

Polarised Fourier-transform infrared (FTIR) absorption spectra were measured on a 35 µm thick doubly polished single-crystal section oriented parallel to the **c**-axis. A Bruker Vertex spectrometer attached to a Hyperion 2000 microscope and equipped with a halogen lamp source, a CaF_2 beamsplitter, a ZnSe wiregrid polariser and an InSb detector was used to collect spectra in the range 2000–13000 cm^{-1} at a resolution of 2 cm^{-1}. Spectra recorded in polarised mode parallel to the crystallographic **c**-axis show a significant band at 3365 cm^{-1}, a very intense band around 3500 cm^{-1}, two weaker bands at 3632 and 3644 cm^{-1}, and two very weak bands at 3662 and 3671 cm^{-1} (Fig. 3). As observed typically for tourmaline spectra in the (OH) range, the main band is off-scale for the **E**||**c** direction due to excessive absorption. Spectra obtained perpendicular to the **c**-axis show considerably weaker bands.

Note that the band at 3365 cm^{-1} is consistent with the presence of minor Al along with Si in [4]-fold coordination (Nishio-Hamane *et al.*, 2014), whereas the comparatively weak

bands above 3600–3650 cm^{-1}, which is the region where bands due to (OH) at the W position ($\equiv$ O1 site) are expected (e.g. Gonzalez-Carreño *et al.*, 1988; Bosi *et al.*, 2015b), indicate small amounts of ^{W}(OH). On the basis of previous investigations of Bosi *et al.* (2012, 2016, 2021) and Watenphul *et al.* (2016), the main broad FTIR band at ~3500 cm^{-1} is probably caused by the occurrence of the atomic arrangements $3[^Y(Mn^{2+}, Al)^ZAl^ZAl]–^{O3}(OH)_3$, whereas the bands above 3600 cm^{-1} may be caused by the arrangements $^Y[(Li,Fe^{2+},Mn^{2+})(Mn^{2+},Al)Al]–^{O1}(OH)–^X(\square)$, where $\square$ = vacancy.

Optical absorption spectroscopy (OAS)

Polarised optical absorption spectra of princivalleite (Fig. 4) were acquired at room temperature on the same polished crystal that was used for the collection of infrared spectra. An AVASPEC-ULS2048X16 spectrometer, connected via a 400 µm UV fibre cable to a Zeiss Axiotron UV-microscope, was used. A 75 W Xenon arc lamp was used as the light source and Zeiss Ultrafluar 10× lenses served as objective and condenser. An UV-quality Glan-Thompson prism, with a working range from 40000 to 3704 cm^{-1} was used as a polariser.

The recorded spectra show two broad absorption bands at 13500 and 8900 cm^{-1}. The weak polarisation of these bands is explained by the absence of Fe^{3+} (e.g. Mattson and Rossman, 1987) in the sample and consequently the bands mark pure *d-d* transitions in [6]-coordinated Fe^{2+}. This assignment agrees with the Fe valency and site distribution observed from Mössbauer spectra of the sample. Additional sharp absorption bands observed in the **E**||**c**-spectrum in the range 6700–7000 cm^{-1} mark overtones of the fundamental (OH)-stretching modes. Weak and relatively sharp absorption bands at ~18000, ~22500, ~24000 and ~27500 cm^{-1} are related to spin-forbidden electronic transitions in [6]-coordinated Mn^{2+} (e.g. Hålenius *et al.*, 2007).

Single-crystal structure refinement

A representative azure crystal of princivalleite from Veddasca Valley was selected for X-ray diffraction measurements on a Bruker KAPPA APEX-II single-crystal diffractometer (Sapienza University of Rome, Earth Sciences Department), equipped with

Table 2. Mössbauer parameters for princivalleite obtained at room-temperature.

| δ (mm/s)	ΔE_Q (mm/s)	FWHM (mm/s)	Area (%)	Assignment
1.09	2.50	0.27	38.1	$^{VI}Fe^{2+}$
1.09	2.19	0.32	28.5	$^{VI}Fe^{2+}$
1.09	1.61	0.41	33.5	$^{VI}Fe^{2+}$

δ = centroid shift, ΔE_Q = quadrupole splitting, FWHM = full width at half-maximum.

a CCD area detector (6.2×6.2 cm active detection area, 512×512 pixels) and a graphite-crystal monochromator, using Mo$K\alpha$ radiation from a fine-focus sealed X-ray tube. The sample-to-detector distance was 4 cm. A total of 1621 exposures (step = 0.4°, time/step = 20 s) covering a full reciprocal sphere with a redundancy of ~12 was collected using ω and φ scan modes. Final unit-cell parameters were refined using the Bruker AXS *SAINT* program on reflections with $I > 10\ \sigma(I)$ in the range 5° < 2θ < 75°. The intensity data were processed and corrected for Lorentz, polarisation and background effects using the *APEX2* software program of Bruker AXS. The data were corrected for absorption using a multi-scan method (*SADABS*, Bruker AXS). The absorption correction led to an improvement in R_{int}. No violation of $R3m$ symmetry was detected.

Structure refinement was done using the *SHELXL-2013* program (Sheldrick, 2015). Starting coordinates were taken from Bosi *et al.* (2015a). The variable parameters were: scale factor, extinction coefficient, atom coordinates, site-scattering values (for *X*, *Y* and *Z* sites) and atomic-displacement factors. The fully ionised-oxygen scattering factor and neutral-cation scattering factors were used. In detail, the *X* site was modelled using the Na scattering factor. The occupancy of the *Y* site was obtained considering the presence of Al *versus* Mn, and the *Z* site with Al *versus* Fe. The *T*, *B* and anion sites were modelled, respectively, with Si, B and O scattering factors and with a fixed occupancy of 1, because refinement with unconstrained occupancies showed no significant deviations from this value. The position of the H atom bonded to the oxygen at the O3 site in the structure was taken from the difference-Fourier map and incorporated into the refinement model; the O3–H3 bond length was restrained (by DFIX command) to be 0.97 Å with the isotropic displacement parameter constrained to be equal to 1.2 times that obtained for the O3 site. There were no correlations greater than 0.7 between the parameters at the end of the refinement. Table 3 lists crystal data, data-collection information, and refinement details; Table 4 gives the fractional atom coordinates, equivalent isotropic-displacement parameters and Table 5 shows selected bond lengths. The crystallographic information file has been deposited with the Principal Editor of *Mineralogical Magazine* and is available as Supplementary material (see below).

Powder X-ray diffraction

A powder X-ray diffraction pattern for princivalleite was collected using a Panalytical X'pert powder diffractometer equipped with an X'celerator silicon-strip detector. The range 5–80° (2θ) was scanned with a step-size of 0.017° with the sample mounted on a background-free Si holder using sample spinning. The diffraction data (for Cu$K\alpha$ = 1.54059 Å), corrected using Si as an internal standard, are listed in Table 6. The program *UnitCell* (Holland and Redfern, 1997) was used to refine unit-cell
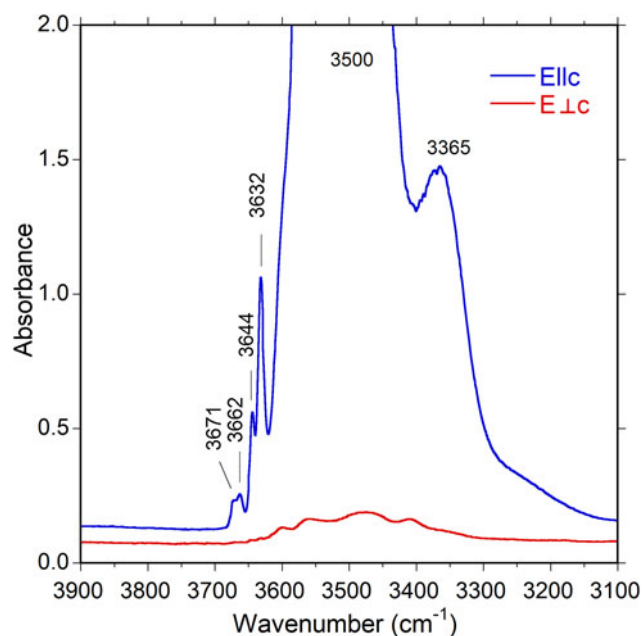
Fig. 3. Polarised FTIR spectra for princivalleite, vertically off-set for clarity. The main band is truncated at ~2 absorbance units in the **E||c** direction due to excessive absorption. Note comparatively low intensities of bands above 3600–3650 cm^{-1} corresponding to very small (OH) contents at W [≡ the O(1) site]. Sample thickness 35 μm.

parameters in the trigonal system: $a = 15.8851(3)$ Å, $c = 7.1041(2)$ Å and $V = 1522.46(5)$ Å^3.

Determination of number of atoms per formula unit (apfu)

In agreement with the structure-refinement results, the boron content was assumed to be stoichiometric (B^{3+} = 3.00 apfu). Both the site-scattering results and the bond lengths of *B* and *T* are consistent with the *B* site being fully occupied by boron and no amount of B^{3+} at the *T* site (e.g. Bosi and Lucchesi, 2007). The iron oxidation state was determined by Mössbauer spectroscopy. In accordance with these results, together with results from optical absorption spectroscopy and Fe and Mn redox potential arguments, all Mn was considered as Mn^{2+}. Lithium was determined by μ-LIBS. The (OH) content and the formula were then calculated by charge balance with the assumption (T + Y + Z) = 15 apfu and 31 anions. The excellent agreement between the number of electrons per formula unit (epfu) derived from EMP data and SREF (223.2 and 223.0 epfu, respectively) supports the stoichiometric assumptions.

Site populations

The princivalleite site populations at the *X*, *B*, *T*, O3 (≡ V) and O1 (≡ W) sites follow the standard site preference suggested for tourmaline (e.g. Henry *et al.*, 2011) and are coherent with the information from FTIR absorption spectra (Fig. 3). In particular, the presence of 0.40 Al apfu at the *T* site is consistent with observed <*T*–O> = 1.624 Å, which is larger than the expected value for <^{T}Si–O> = 1.619(1) Å (Bosi and Lucchesi, 2007). The site populations at the octahedrally coordinated *Y* and *Z* sites were optimised according to the procedure of Bosi *et al.* (2017), and by fixing the minor elements Zn and Li at the *Y* site.
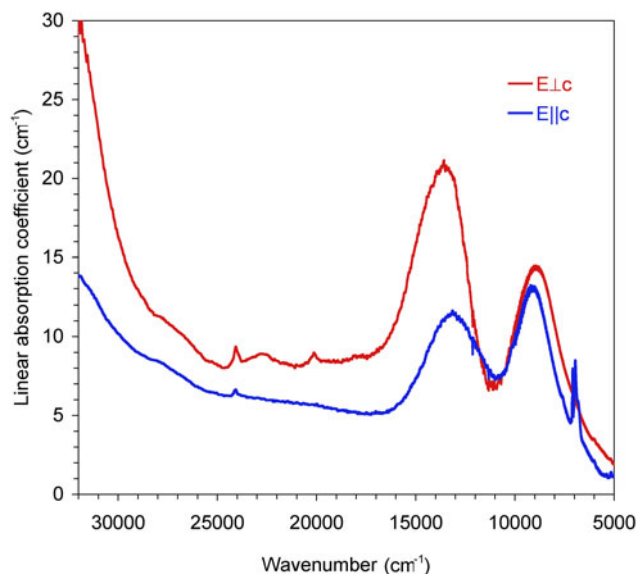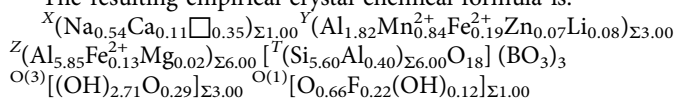
Fig. 4. Polarised optical absorption spectra of princivalleite in the UV and visible region.

Table 3. Single-crystal X-ray diffraction data details for princivalleite.

Crystal data

Space group	$R3m$
a (Å)	15.9155(2)
c	7.11660(10)
V (Å^3)	1561.15(4)
Z	3
Density (calc) (g/cm^3)	3.168
Reciprocal space range hkl	$-26 \leq h \leq 22; -27 \leq k \leq 26; -8 \leq l \leq 11$
Data collection	
Crystal size (mm)	0.14 × 0.28 × 0.32
Data collection temperature (K)	293
Radiation, λ	Mo$K\alpha$, 0.71073 Å
Axis, frame width (°), time per frame (s)	Phi-omega, 0.4, 20
Range for data collection, 2θ (°)	5–75
Set of read reflections	11559
Unique reflections, R_{int} (%)	1758, 1.72
Unique reflections with $I > 2\sigma(I)$	1744
Redundancy	12
Absorption correction method	Multiscan (*SADABS*)
Refinement	
Refinement method	Full-matrix last-squares on F^2
Structural refinement program	*SHELXL–2013*
Restraints, refined parameters	1, 94
Extinction coefficient	0.0004(1)
Flack parameter	–0.06(3)
wR_2 (%)	3.22
R_1 (%) all data	1.36
R_1 (%) for $I > 2\sigma_I$	1.34
GooF	1.098
$\Delta\rho_{max}, \Delta\rho_{min}$ (e^-/Å^3)	–0.34 and 0.76

Notes: R_{int} = merging residual value; R_1 = discrepancy index, calculated from F-data; wR_2 = weighted discrepancy index, calculated from F^2-data; GooF = goodness of fit. Refined as an inversion twin.

The resulting empirical crystal-chemical formula is:

^{X}(Na$_{0.54}$Ca$_{0.11}$□$_{0.35}$)$_{\Sigma1.00}$ ^{Y}(Al$_{1.82}$Mn$^{2+}_{0.84}$Fe$^{2+}_{0.19}$Zn$_{0.07}$Li$_{0.08}$)$_{\Sigma3.00}$ ^{Z}(Al$_{5.85}$Fe$^{2+}_{0.13}$Mg$_{0.02}$)$_{\Sigma6.00}$ [^{T}(Si$_{5.60}$Al$_{0.40}$)$_{\Sigma6.00}$O$_{18}$] (BO$_3$)$_3$ $^{O(3)}$[(OH)$_{2.71}$O$_{0.29}$]$_{\Sigma3.00}$ $^{O(1)}$[O$_{0.66}$F$_{0.22}$(OH)$_{0.12}$]$_{\Sigma1.00}$

A comparison between the values of refined site-scatterings and those calculated from this site population is reported in

Table 4. Fractional atom coordinates, isotropic (*) or equivalent-isotropic displacement parameters (in Å^2) and site occupancy factors (s.o.f.) for princivalleite.

	x/a	y/b	z/c	$U_{eq/iso}$	s.o.f.
X	0	0	0.2186(3)	0.0183(6)	Na$_{0.768(8)}$
Y	0.12317(3)	0.06158(2)	0.62913(8)	0.00924(12)	Mn$_{0.344(4)}$Al$_{0.656(4)}$
Z	0.29764(2)	0.26108(2)	0.60857(7)	0.00545(9)	Al$_{0.985(2)}$Fe$_{0.015(2)}$
B	0.10971(6)	0.21942(12)	0.4520(3)	0.0062(3)	B$_{1\cdot00}$
T	0.19197(2)	0.18996(2)	0	0.00469(7)	Si$_{1\cdot00}$
O(1) ≡ W	0	0	0.7733(4)	0.0289(7)	O$_{1\cdot00}$
O(2)	0.06103(5)	0.12205(9)	0.4846(2)	0.0157(3)	O$_{1\cdot00}$
O(3) ≡ V	0.26500(11)	0.13250(5)	0.5073(2)	0.0114(2)	O$_{1\cdot00}$
H(3)	0.2565(19)	0.1283(10)	0.380(3)	0.014*	H$_{1\cdot00}$
O(4)	0.09386(5)	0.18772(9)	0.0713(2)	0.0093(2)	O$_{1\cdot00}$
O(5)	0.18717(10)	0.09358(5)	0.09383(19)	0.0100(2)	O$_{1\cdot00}$
O(6)	0.19638(6)	0.18578(6)	0.77343(14)	0.00715(14)	O$_{1\cdot00}$
O(7)	0.28642(6)	0.28643(5)	0.07758(13)	0.00596(14)	O$_{1\cdot00}$
O(8)	0.20951(6)	0.27036(6)	0.43803(14)	0.00699(15)	O$_{1\cdot00}$

*Isotropic displacement parameters (U_{iso}) for H(3) constrained to have a U_{iso} 1.2 times the U_{eq} value of the O(3) oxygen atom.

Table 5. Selected bond lengths (Å) for princivalleite.

X–O2 × 3	2.533(2)	B–O2	1.362(2)	Z–O6	1.8651(9)
X–O5 × 3	2.7283(15)	B–O8 × 2	1.3791(12)	Z–O7	1.8754(9)
X–O4 × 3	2.7916(16)	<B–O>	1.373	Z–O8	1.8858(9)
<X–O>	2.684			Z–O8$'$	1.9155(9)
		T–O7	1.6167(8)	Z–O7$'$	1.9428(9)
Y–O2 × 2	1.9783(10)	T–O6	1.6168(10)	Z–O3	1.9784(7)
Y–O1	1.9837(16)	T–O4	1.6252(5)	<Z–O>	1.911
Y–O6 × 2	2.0040(9)	T–O5	1.6393(6)		
Y–O3	2.1386(15)	<T–O>	1.624		
<Y–O>	2.014				

Table 7. The agreement between the refined and calculated values is very good, and validates the distribution of cations over the X, Y, Z and T sites in the empirical structural formula of princivalleite. This site population is also supported by the comparison of weighted bond valence sums and mean formal charge calculated from the empirical structural formula (Table 8).

For classification purposes, the empirical crystal-chemical formula was recast in its ordered form following Henry *et al.* (2011):

^{X}(Na$_{0.54}$Ca$_{0.11}$□$_{0.35}$)$_{\Sigma1.00}$ ^{Y}(Al$_{1.67}$Mn$^{2+}_{0.84}$Fe$^{2+}_{0.32}$Zn$_{0.07}$Mg$_{0.02}$Li$_{0.08}$)$_{\Sigma3.00}$ ^{Z}Al$_6$ ^{T}[(Si$_{5.60}$Al$_{0.40}$)$_{\Sigma6.00}$O$_{18}$] (BO$_3$)$_3$ ^{V}[(OH)$_{2.71}$O$_{0.29}$]$_{\Sigma3.00}$ ^{W}[O$_{0.66}$F$_{0.22}$(OH)$_{0.12}$]$_{\Sigma1.00}$.

End-member formula and relation to other species

The composition of the present sample is consistent with an oxy-tourmaline belonging to the alkali group (Henry *et al.*, 2011): it is Na-dominant at the X position of the general formula of tourmaline, oxy-dominant at W with O^{2-} > (F + OH) and Al^{3+} dominant at Z.

With regard to the Y position, the formula electroneutrality requires that the total charge at Y is +7 in the end-member formula: Na(Y_3)$^{\Sigma7+}$Al$_6$(Si$_6$O$_{18}$)(BO$_3$)$_3$(OH)$_3$O. In accord with the dominant-valency rule and the valency-imposed double site-occupancy (Bosi *et al.*, 2019a, 2019b), the possible charge and atomic arrangements compatible with the Y-site population in the ordered formula are:

Table 6. Powder X-ray diffraction patterns for princivalleite.

I (%)	d_{meas} (Å)	d_{cal} (Å)	h	k	l
24	6.315	6.312	1	0	1
16	4.945	4.942	0	2	1
9	4.588	4.586	0	3	0
43	**4.198**	**4.196**	**2**	**1**	**1**
50	**3.974**	**3.971**	**2**	**2**	**0**
67	**3.441**	**3.439**	**0**	**1**	**2**
10	3.361	3.361	1	3	1
9	3.003	3.002	1	4	0
78	**2.934**	**2.933**	**1**	**2**	**2**
6	2.885	2.884	3	2	1
6	2.601	2.600	3	1	2
100	**2.567**	**2.566**	**0**	**5**	**1**
19	2.368	2.368	0	0	3
17	2.359	2.359	2	3	2
18	2.334	2.334	5	1	1
13	2.175	2.175	5	0	2
14	2.156	2.155	4	3	1
22	2.103	2.104	3	0	3
30	2.034	2.034	2	2	3
51	**2.028**	**2.028**	**1**	**5**	**2**
8	2.012	2.012	1	6	1
41	1.908	1.908	3	4	2
11	1.859	1.859	1	4	3
9	1.843	1.842	6	2	1
10	1.764	1.765	3	3	3
7	1.720	1.720	0	2	4
7	1.681	1.681	2	6	2
34	1.647	1.647	0	6	3
19	1.589	1.589	5	5	0
11	1.578	1.578	4	0	4
8	1.541	1.540	4	6	1
6	1.529	1.529	0	9	0
5	1.519	1.519	7	2	2
25	1.492	1.492	0	5	4
7	1.467	1.466	2	4	4
34	1.442	1.442	5	1	4
18	1.413	1.413	6	5	1
25	1.397	1.399	6	3	3
11	1.351	1.351	10	0	1
5	1.336	1.336	9	1	2
6	1.318	1.318	7	0	4
13	1.306	1.306	10	1	0
6	1.300	1.300	8	3	2
5	1.272	1.272	9	3	0
21	1.262	1.262	5	0	5
5	1.232	1.232	0	11	1

Notes: only the reflections with $I \geq 5\%$ are listed. The six strongest reflections are given in bold.

$$^Y(2^+_2 3^+)^{\Sigma 7+} \rightarrow {}^Y(2^+_2 3^+)_{0.625} \rightarrow (2^+_{1.250}Al^{3+}_{0.625}) = 1.875 \text{ apfu (limited by } 2^+ \text{ contents)}$$

$$^Y(3^+_2 1^+)^{\Sigma 7+} \rightarrow {}^Y(3^+_2 1^+)_{0.080} \rightarrow (Al^{3+}_{0.160}Li^+_{0.080}) = 0.240 \text{ apfu (limited by Li contents)}$$

As a result, and in accordance with the dominant-valency rule, the proportion of the arrangement $(2^+_{1.250}Al^{3+}_{0.625})$ is greater than the proportion of $(Al^{3+}_{0.160}Li^+_{0.080})$. In accordance with the dominant-constituent rule, Mn^{2+} prevails among the 2^+-cations (0.84 Mn apfu > 0.32 Fe > 0.07 Zn > 0.02 Mg). Thus, the atomic arrangement $(Mn^{2+}_2 Al^{3+})$ is the dominant one: $(Mn^{2+}_2 Al^{3+})_{0.42} = 1.26$ apfu. The end-member composition may hence be represented as $Na(Mn_2Al)Al_6(Si_6O_{18})(BO_3)_3(OH)_3O$. As no tourmalines are currently approved with this composition, it can be identified as a new species.

Princivalleite is related to oxy-schorl and darrellhenryite by the substitutions $Mn^{2+} \leftrightarrow Fe^{2+}$ and $2Mn^{2+} \leftrightarrow Al^{3+} + Li^+$. The

Table 7. Refined site-scattering values and optimised site-populations for princivalleite.

Site	Refined site-scattering (epfu)	Optimized site-population (apfu)	Calculated site-scattering (epfu)
X	8.45(7)	0.54 Na + 0.11 Ca + 0.35 □	8.12
Y	51.38(21)	1.82 Al + 0.84 Mn^{2+} + 0.19 Fe^{2+} + 0.07 Zn + 0.08 Li	51.84
Z	79.17(24)	5.85 Al + 0.13 Fe^{2+} + 0.02 Mg	79.67

Table 8. Weighted bond valences (valence units) for princivalleite.

Site	X	Y	Z	T	B	Σ_{anion}
O(1)		$^{3\times\rightarrow}$0.46				1.38
O(2)	0.10$^{\downarrow 3}$	$^{2\times\rightarrow}$0.47$^{\downarrow\times2}$			1.02	2.06
O(3)		0.31	$^{2\times\rightarrow}$0.43			1.16
O(4)	0.05$^{\downarrow 3}$			$^{2\times\rightarrow}$1.00		2.04
O(5)	0.06$^{\downarrow 3}$			$^{2\times\rightarrow}$0.96		1.98
O(6)		0.44$^{\downarrow\times2}$	0.56	1.02		2.02
O(7)			0.55	1.02		2.02
			0.46			
O(8)			0.49		0.98$^{\downarrow\times2}$	2.00
			0.53			
Σ_{cation}	0.62	2.58	3.01	4.00	2.98	
MFC[a]	0.76	2.58	2.97	3.93	3.00	

Note: Weighted bond valence according to Bosi (2014). Bond valence parameters from Brown and Altermatt (1985).
[a]Mean Formal Charge (or weighted atomic valence) from the empirical crystal-chemical formula.

properties of these three tourmalines are compared in Table 9, whereas the position of the princivalleite holotype sample in the ternary diagram for the $(Fe^{2+}_2 Al)$–$(Mn^{2+}_2 Al)$–$(Al_2 Li)$ subsystem is displayed in Fig. 5. This figure also shows the chemical variability of princivalleite to oxy-schorl and darrellhenryite by the occurrence of two additional samples from the same batch of tourmalines from the Veddasca rock sample (Fig. 1) and samples from Uvildy, Chelyabinsk region, Russia, and Pikárec, Czech Republic (Cempírek et al., 2015; Bosi et al., 2022). The chemical composition of these four samples is reported in Table 10. Moreover, the chemical composition of the yellow Mn-tourmaline identified as tsilaisite by Nuber and Schmetzer (1984) is ^{W}O-dominant; thus, it corresponds to princivalleite (Fig. 5). It is most likely that the locality of this yellow tourmaline should be the Canary mining area in the Lundazi District of eastern Zambia (for details, see Laurs et al., 2007), although it is important to point out that other tourmalines from this locality are actually Mn-rich elbaite or fluor-elbaite samples (Laurs et al., 2007; Simmons et al., 2011).

Petrogenesis of princivalleite

Formation of Mn-dominant tourmalines (e.g. tsilaisite, fluor-tsilaisite and celleriite; Bosi et al., 2012, 2015a, 2022) requires specific geochemical conditions that are rare in nature: ideally, high activity of Al and Mn combined with low activity of Fe, Li and Mg. For example, Simmons et al. (2011) suggested that the original pegmatite-forming melt (preferably a B-rich peraluminous melt) of tsilaisitic and Mn-rich elbaite tourmalines

Table 9. Comparative data for princivalleite, oxy-schorl and darrellhenryite.

	Princivalleite[a]	Oxy-schorl[b]	Darrellhenryite[c]
a (Å)	15.9155(2)	15.916(3)	15.809(2)
c (Å)	7.1166(1)	7.107(1)	7.089(1)
V (Å^3)	1561.15(4)	1559.1(4)	1534.4(4)
Space group	$R3m$	$R3m$	$R3m$
Optic sign	Uniaxial (–)	Uniaxial (–)	Uniaxial (–)
ω	1.650(5)	1.663(2)	1.636(2)
ε	1.635(5)	1.641(2)	1.619(2)
Streak	White	Pale gray	White
Colour	Azure	Greenish black	Pink
Pleochroism in thin section	Colourless	O = green to bluish-green	Colourless
		E = pale yellowish to nearly colourless	
Strong lines in the powder XRD pattern d(Å) (I, %)	2.567 (100)	3.466 (100)	2.925 (100)
	2.934 (78)	2.955 (79)	2.555 (90)
	3.441 (67)	6.364 (75)	3.431 (73)
	2.028 (51)	2.583 (65)	3.952 (54)
	3.974 (50)	3.997 (52)	1.901 (50)
	4.198 (43)	4.225 (48)	1.643 (49)
Reference	This work	Bačík *et al.* (2013)	Novák *et al.* (2013)

[a]Na(Mn$_2$Al)Al$_6$(Si$_6$O$_{18}$)(BO$_3$)$_3$(OH)$_3$O
[b]Na(Fe$_2$Al)Al$_6$(Si$_6$O$_{18}$)(BO$_3$)$_3$(OH)$_3$O
[c]Na(LiAl$_2$)Al$_6$(Si$_6$O$_{18}$)(BO$_3$)$_3$(OH)$_3$O
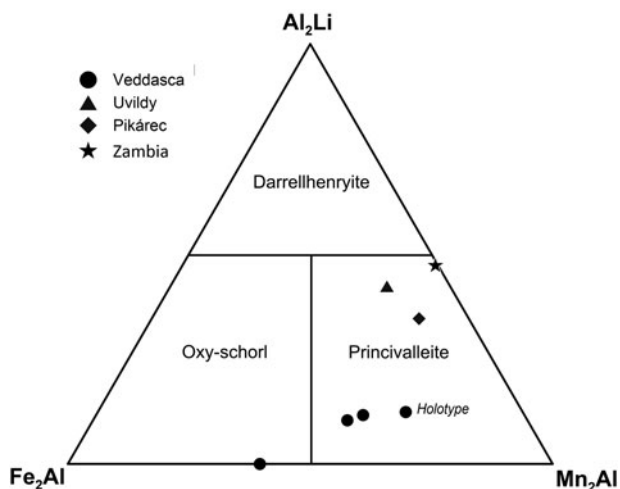
Fig. 5. Plot of princivalleite compositions on the (Fe$_2^{2+}$Al)–(Mn$_2^{2+}$Al)–(Al$_2$Li) diagram. Black circles represent the coexisting samples from same batch of tourmalines from the Veddasca rock sample (Italy); black triangle and black diamond represent princivalleite samples from Uvildy (Russia) and Pikárec (Czech Republic), respectively; black star is the yellow Mn-tourmaline from Zambia (Nuber and Schmetzer, 1984) identified as princivalleite in this study.

must be relatively low in Fe and enriched in Mn and B, moreover, during the early stages of crystallisation Fe must be removed, but abundant B and Mn must still be available when tourmaline crystallises.

The system, at the stage of growth of princivalleite, must be also depleted in F; this condition is not commonly achieved as Mn-enrichment in pegmatites is typically followed by an increase of F content in the system and in the Mn-rich tourmalines formed (e.g. Selway *et al.*, 1999; Dixon *et al.*, 2014). Manganese enrichment in late-stage pocket tourmaline is a characteristic feature of elbaite-subtype pegmatites (e.g., Novák and Povondra, 1995; Novotný and Cempírek, 2021; Bosi *et al.*, 2022) that, compared to lepidolite-subtype (Selway *et al.*, 1999) or transitional

pegmatites (Dixon *et al.*, 2014; Roda-Robles *et al.*, 2015), contain lower amounts of F. The latter typically remains below 0.5 apfu in tourmaline until the hydrothermal-metasomatic stage of pegmatite crystallisation, which is characterised by fluor-elbaite to fluor-liddicoatite compositions (e.g. Novotný and Cempírek, 2021; Zahradníček, 2012; Flégr, 2016). This is the case of the princivalleite occurrences in the Uvildy and Pikárec pegmatites (Table 10), whereas F in princivalleite from Veddasca valley could have been limited by the abundant crystallisation of muscovite in the pegmatitic vein.

Princivalleite from Veddasca Valley is Li-poor and relatively Fe^{2+}-rich, with Fe^{2+} contents that are sometimes higher than those of Mn^{2+}, leading to the oxy-schorl compositions. Despite princivalleite being an oxy-species, the occurrence of Mn and Fe in oxidation state +2 indicates that its formation is not constrained by oxidising conditions. Princivalleite originated in a B-rich and peraluminous anatectic pegmatitic melt formed *in situ*, poor in Fe and characterised by reducing conditions, as evidenced by the occurrence of rare pyrite and only Fe^{2+} in tourmaline. Such reducing conditions are related to a low fugacity of oxygen in the late-stage metamorphic fluids derived by the flaser gneiss, which promoted the formation of very low levels of melting. The formation of this type of vein could also be compatible with the crystallisation of batches of 'silicate-rich fluids', as in the model proposed by Thomas and Davidson (2012). The Mn-enrichment in tourmaline was allowed by the lack of formation other minerals competing for this element such as garnet.

The Mn-enrichment is unusual for anatectic pegmatites (cf. Cempírek and Novák 2006, Cempírek *et al.* 2006); we therefore assume that micas (especially biotite) in the protolith metapelite were enriched in Mn, possibly due to admixture of volcanosedimentary component; this might also be indicated by relatively elevated ZnO contents in princivalleite (Tables 1 and 10). Another explanation might be an unexposed magmatic source of melt as in the case of (apparently anatectic) kyanite-bearing Li-rich pegmatites at Virorco, Argentina (Galliski *et al.* 2012).

Table 10. Chemical composition of princivalleite (Prn) and oxy-schorl (Osch) from: Veddasca Valley, Varese, Lombardy, Italy; Uvildy, Chelyabinsk region, Russia; and Pikárec, Czech Republic.

	Prn-V7 Veddasca (n = 4)	Prn-V4 Veddasca (n = 7)	Osch Veddasca (n = 13)	Prn Uvildy (n = 8)	Prn Pikárec (n = 4)
Wt.%					
SiO_2	34.32(64)	34.41(46)	32.86(70)	34.44(28)	35.38(9)
B_2O_3[a]	10.53	10.60	10.33	10.64	10.61
Al_2O_3	42.19(79)	41.46(27)	39.73(41)	42.97(64)	39.64(11)
FeO	2.71(61)	3.79(12)	6.63(28)	1.29(12)	1.37(31)
MnO	4.43(24)	5.28(14)	4.29(19)	4.36(41)	7.36(15)
MgO	0.22(24)	0.08(3)	–	0.15(11)	–
ZnO	0.41(5)	0.22(6)	0.44(5)	–	0.22(4)
CaO	0.51(11)	0.72(6)	0.59(4)	0.10(3)	0.04(3)
Na_2O	1.74(1)	1.71((5)	1.78(3)	1.73(7)	1.84(16)
Li_2O	0.12(1)[b]	0.11(4)[b]	–	0.43(5)[c]	0.48(6)[c]
F	0.40(13)	0.40(11)	0.50(7)	0.40(11)	0.46(7)
H_2O[a]	2.36	2.53	2.69	2.73	2.95
$-O \equiv F$	–0.17	–0.17	–0.21	–0.17	–0.19
Total	99.89	101.19	99.63	99.08	100.17
Ordered formula					
^{T}Si (apfu)	5.65	5.63	5.53	5.63	5.80
^{T}Al	0.35	0.37	0.47	0.37	0.20
ΣT	6.00	6.00	6.00	6.00	6.00
^{B}B	3.00	3.00	3.00	3.00	3.00
^{Z}Al	6.00	6.00	6.00	6.00	6.00
^{Y}Al	1.83	1.63	1.40	1.90	1.44
^{Y}Fe^{2+}	0.37	0.52	0.93	0.18	0.19
^{Y}Mn^{2+}	0.62	0.73	0.61	0.60	1.02
^{Y}Mg	0.05	0.02	0.00	0.04	0.00
^{Y}Zn	0.05	0.03	0.06	0.00	0.03
^{Y}Li	0.08	0.07	0.00	0.29	0.32
ΣY	3.00	3.00	3.00	3.00	3.00
^{X}Ca	0.09	0.13	0.11	0.02	0.01
^{X}Na	0.55	0.54	0.58	0.55	0.58
$^X\square$	0.36	0.33	0.32	0.43	0.41
ΣX	1.00	1.00	1.00	1.00	1.00
^{V}(OH)	2.67	2.81	3.00	2.98	3.00
^{V}O	0.33	0.19	0.00	0.02	0.00
ΣV	3.00	3.00	3.00	3.00	3.00
^{W}F	0.21	0.21	0.28	0.20	0.24
^{W}O	0.79	0.79	0.71	0.80	0.51
^{W}(OH)	0.00	0.00	0.01	0.00	0.25
ΣW	1.00	1.00	1.00	1.00	1.00

Atoms per formula unit (apfu) normalised to 31 anions. Standard deviations for oxides and F are in brackets.
[a]Calculated by stoichiometry (see text). [b]Determined by μ-LIBS. [c]Determined by LA-ICP-MS. '–' = below detection limits

References

Bačík P. and Fridrichová G. (2020) Cation partitioning among crystallographic sites based on bond-length constraints in tourmaline-supergroup minerals. *American Mineralogist,* https://doi.org/10.2138/am-2021-7804

Bačík P., Cempírek J., Uher P., Novák M., Ozdín D., Filip J., Škoda R., Breiter K., Klementová M. and Ďuďa R. (2013) Oxy-schorl, Na(Fe$_2^{2+}$Al) Al$_6$Si$_6$O$_{18}$(BO$_3$)$_3$(OH)$_3$O, a new mineral from Zlatá Idka, Slovak Republic and Přibyslavice, Czech Republic. *American Mineralogist*, **98**, 485–492.

Boriani A., Giobbi Origoni E. and Borghi A. (1990) The evolution of the "Serie dei Laghi" (Strona Ceneri and Scisti dei Laghi): the upper component of the Ivrea Verbano crustal section; Southern Alps, North Italy and Ticino, Switzerland. *Tectonophysics*, **82**, 103–118.

Bosi F. (2013) Bond-valence constraints around the O1 site of tourmaline. *Mineralogical Magazine*, **77**, 343–351.

Bosi F. (2014) Bond valence at mixed occupancy sites. I. Regular polyhedra. *Acta Crystallographica*, **B70**, 864–870.

Bosi F. (2018) Tourmaline crystal chemistry. *American Mineralogist*, **103**, 298–306.

Bosi F. and Lucchesi S. (2007) Crystal chemical relationships in the tourmaline group: structural constraints on chemical variability. *American Mineralogist*, **92**, 1054–1063.

Bosi F., Skogby H., Agrosì G. and Scandale E. (2012) Tsilaisite, NaMn$_3$Al$_6$(Si$_6$O$_{18}$)(BO$_3$)$_3$(OH)$_3$OH, a new mineral species of the tourmaline supergroup from Grotta d'Oggi, San Pietro in Campo, island of Elba, Italy. *American Mineralogist*, **97**, 989–994.

Bosi F., Andreozzi G.B., Agrosì G. and Scandale E. (2015a) Fluor-tsilaisite, NaMn$_3$Al$_6$(Si$_6$O$_{18}$)(BO$_3$)$_3$(OH)$_3$F, a new tourmaline from San Piero in Campo (Elba, Italy) and new data on tsilaisitic tourmaline from the holo-type specimen locality. *Mineralogical Magazine*, **79**, 89–101.

Bosi F., Skogby H., Lazor P., Reznitskii L. (2015b) Atomic arrangements around the O3 site in Al- and Cr-rich oxy-tourmalines: a combined EMP, SREF, FTIR and Raman study. *Physics and Chemistry of Minerals*, **42**, 441–453.

Bosi F., Skogby H. and Balić-Žunić T. (2016) Thermal stability of extended clusters in dravite: a combined EMP, SREF and FTIR study. *Physics and Chemistry of Minerals*, **43**, 395–407.

Bosi F., Reznitskii L., Hålenius U. and Skogby H. (2017) Crystal chemistry of Al–V–Cr oxy-tourmalines from Sludyanka complex, Lake Baikal, Russia. *European Journal of Mineralogy*, **29**, 457–472.

Bosi F., Biagioni C. and Oberti R. (2019a) On the chemical identification and classification of minerals. *Minerals*, **9**, 591.

Bosi F., Hatert F., Hålenius U., Pasero M., Miyawaki R., and Mills S.J. (2019b) On the application of the IMA-CNMNC dominant-valency rule to complex mineral compositions. *Mineralogical Magazine*, **83**, 627–632.

Bosi F., Pezzotta F., Skogby H., Altieri A., Hålenius U., Tempesta G. and Cempírek J. (2020) Princivalleite, IMA 2020-056. CNMNC Newsletter No. 58. *Mineralogical Magazine*, **84**, 971–975, doi:https://doi.org/10.1180/mgm.2020.93.

Bosi F., Celata B., Skogby H., Hålenius U., Tempesta G., Ciriotti M.E., Bittarello E., Marengo A. (2021) Mn-bearing purplish-red tourmaline from the Anjanabonoina pegmatite, Madagascar. *Mineralogical Magazine*, **85**, 242–253.

Bosi F., Pezzotta F., Altieri A., Andreozzi G.B., Ballirano P., Tempesta G., Cempírek J., Škoda R., Filip J., Čopjaková R., Novák M., Kampf A.R., Scribner E.D., Groat L.A. and Evans R.J. (2022) Celleriite, $\square$ (Mn$_2^{2+}$Al) Al$_6$(Si$_6$O$_{18}$)(BO$_3$)$_3$(OH)$_3$(OH), a new mineral species of the tourmaline supergroup. *American Mineralogist*, **107**, 31–42.

Brown D. and Altermatt D. (1985) Bond-valence parameters obtained from a systematic analysis of the Inorganic Crystal Structure Database. *Acta Crystallographica,* **B41**, 244–247.

Cempírek J. and Novák M. (2006) Mineralogy of dumortierite-bearing abyssal pegmatites at Starkoč and Běstvina, Kutná Hora Crystalline Complex. *Journal of the Czech Geological Society*, **51**, 3–4.

Cempírek J., Novák M., Ertl A., Hughes J.M., Rossman G.R. and Dyar M.D. (2006) Fe-bearing olenite with tetrahedrally coordinated Al from an abyssal pegmatite at Kutná Hora, Czech Republic: structure, crystal chemistry, optical and XANES spectra. *The Canadian Mineralogist*, **44**, 23–30.

Cempírek J., Houzar S., Novák M., Groat L.A., Selway J.B. and Šrein V. (2013) Crystal structure and compositional evolution of vanadium-rich oxy-dravite from graphite quartzite at Bítovánky, Czech Republic. *Journal of Geosciences*, **58**, 149–162.

Cempírek J., Groat L.A., Scott G.C., Novák M. and Škoda R. (2015) Deformed Li-pegmatite with dumortierite from Uvildy, Russia. Pp. 14–15 in: *Book of Abstracts, Proceedings of the 7th International Symposium on Granitic Pegmatites PEG 2015, Ksiaz, Poland, 17–19 June 2015.* Tigris, Zlín, Czech Republic.

Dixon A., Cempírek J. and Groat L.A. (2014) Mineralogy and geochemistry of pegmatites on Mount Begbie, British Columbia. *The Canadian Mineralogist*, **52**, 129–164.

Ertl A., Hughes J.M., Pertlik F., Foit F.F. Jr., Wright S.E., Brandstatter F. and Marler B. (2002) Polyhedron distortions in tourmaline. *The Canadian Mineralogist*, **40**, 153–162.

Flégr T. (2016) *Vývoj chemického složení turmalínů z elbaitového pegmatitu Řečice.* M.S. thesis, Faculty of Science, Masaryk University, Brno, Czech Republic [in Czech].

Foit F.F. Jr. (1989) Crystal chemistry of alkali-deficient schorl and tourmaline structural relationships. *American Mineralogist*, **74**, 422–431.

Galliski M.A., Marquez-Zavalia M.F., Lira R., Cempírek J. and Škoda R. (2012) Mineralogy and origin of the dumortierite-bearing pegmatites of Virorco, San Luis, Argentina. *The Canadian Mineralogist*, **50**, 873–894.

Gonzales-Carreño T., Fernández M. and Sanz J. (1988) Infrared and electron microprobe analysis of tourmaline. *Physics and Chemistry of Minerals*, **15**, 452–460.

Hålenius U Bosi F. and Skogby H. (2007) Galaxite, $MnAl_2O_4$, a spectroscopic standard for tetrahedrally coordinated Mn^{2+} in oxygen-based mineral structures. *American Mineralogist*, **92**, 1225–1231.

Hawthorne F.C. (1996) Structural mechanisms for light-element variations in tourmaline. *The Canadian Mineralogist*, **34**, 123–132.

Hawthorne F.C. and Henry D. (1999) Classification of the minerals of the tourmaline group. *European Journal of Mineralogy*, **11**, 201–215.

Henry D.J. and Dutrow B.L. (2011) The incorporation of fluorine in tourmaline: Internal crystallographic controls or external environmental influences? *The Canadian Mineralogist*, **49**, 41–56.

Henry D.J., Novák M., Hawthorne F.C., Ertl A., Dutrow B., Uher P. and Pezzotta F. (2011) Nomenclature of the tourmaline supergroup minerals. *American Mineralogist*, **96**, 895–913.

Holland T.J.B. and Redfern S.A.T. (1997) Unit cell refinement from powder diffraction data: the use of regression diagnostics. *Mineralogical Magazine*, **61**, 65–77.

Laurs B.M., Simmons W.B., Rossman G.R., Fritz E.A., Koivula J.I., Anckar B. and Falster A.U. (2007) Yellow Mn-rich tourmaline from the Canary mining area, Zambia. *Gems and Gemology*, **43**, 314–331.

Mandarino J.A. (1981) The Gladstone-Dale relationship. Part IV: the compatibility concept and its application. *The Canadian Mineralogist*, **19**, 441–450.

Mattson S.M and Rossman G.R. (1987) Fe^{2+}-Fe^{3+} interactions in tourmaline. *Physics and Chemistry of Minerals*, **14**, 163–171.

Nishio-Hamane D., Minakawa T., Yamaura J., Oyama T., Ohnishi M. and Shimobayashi N. (2014) Adachiite, a Si-poor member of the tourmaline supergroup from the Kiura mine, Oita Prefecture, Japan. *Journal of Mineralogical and Petrological Sciences*, **109**, 74–78.

Novák M. and Povondra P. (1995) Elbaite pegmatites in the Moldanubicum: a new subtype of the rare-element class. *Mineralogy and Petrology*, **55**, 159–176.

Novák M., Povondra P. and Selway J.B. (2004) Schorl–oxy-schorl to dravite-oxydravite tourmaline from granitic pegmatites; examples from the Moldanubicum, Czech Republic. *European Journal of Mineralogy*, **16**, 323–333.

Novák M., Ertl A., Povondra P., Galiová M.V., Rossman G.R., Pristacz H., Prem M., Giester G., Gadas P. and Škoda R. (2013) Darrellhenryite, Na $(LiAl_2)Al_6(BO_3)_3Si_6O_{18}(OH)_3O$, a new mineral from the tourmaline supergroup. *American Mineralogist*, **98**, 1886–1892.

Novotný F. and Cempírek J. (2021) Mineralogy of the elbaite-subtype pegmatite from Dolní Rožínka. *Acta Musei Moraviae, Scientiae Geologicae*, **106**, 1, 3–33.

Nuber B. and Schmetzer K. (1984) Structural refinement of tsilaisite (manganese tourmaline). *Neues Jahrbuch für Mineralogie, Monatshefte*, **7**, 301–304.

Pesquera A., Gil-Crespo P.P Torres-Ruiz F., Torres-Ruiz J. and Roda-Robles E. (2016) A multiple regression method for estimating Li in tourmaline from electron microprobe analyses. *Mineralogical Magazine*, **80**, 1129–1133.

Pezzotta F. and Pinarelli L. (1994) The magmatic evolution of Ordovician metagranitoids of the Serie dei Laghi (Southern Alps); inferences from petrological, geochemical, and Sr and Nd isotope data. *Periodico di Mineralogia*, **63**, 127–147.

Pouchou J.L. and Pichoir F. (1991) Quantitative analysis of homogeneous or stratified microvolumes applying the model "PAP". Pp. 31–75 in: *Electron Probe Quantitation* (K.F.J. Heinrich and D.E. Newbury, editors). Plenum, New York.

Prescher C., McCammon C. and Dubrowinsky L. (2012) *MossA*: a program for analyzing energy-domain Mössbauer spectra from conventional and synchrotron sources. *Journal of Applied Crystallography*, **45**, 329–331.

Roda-Robles E., Simmons W., Pesquera A., Gil-Crespo P.P., Nizamoff J. and Torres-Ruiz J. (2015) Tourmaline as a petrogenetic monitor of the origin and evolution of the Berry-Havey pegmatite (Maine, USA). *American Mineralogist*, **100**, 95–109.

Selway J.B., Novák M., Černý P. and Hawthorne F.C. (1999) Compositional evolution of tourmaline in lepidolite-subtype pegmatites. *European Journal of Mineralogy*, **11**, 569–584.

Sheldrick G.M. (2015) Crystal structure refinement with SHELXL. *Acta Crystallographica*, **C71**, 3–8.

Simmons W.B., Falster A.U. and Laurs B.M. (2011) A survey of Mn-rich yellow tourmaline from worldwide localities and implications for the petrogenesis of granitic pegmatites. *The Canadian Mineralogist*, **49**, 301–319.

Thomas R. and Davidson P. (2012) Water in granite and pegmatite-forming melts. *Ore Geology Reviews*, **46**, 32–46.

Watenphul A., Burgdorf M., Schlüter J., Horn I., Malcherek T. and Mihailova B. (2016) Exploring the potential of Raman spectroscopy for crystallochemical analyses of complex hydrous silicates: II. Tourmalines. *American Mineralogist*, **101**, 970–985.

Zahradníček L. (2012) *Vývoj textur a chemického složení zonálních turmalínů z elbaitového pegmatitu v Pikárci u Křižanova.* M.S. thesis, Faculty of Science, Masaryk University, Brno, Czech Republic [in Czech].